The Astrophysical Journal Letters, 866:L23 (7pp), 2018 October 20 https://doi.org/10.3847/2041-8213/aae529

Dust Motions in Magnetized Turbulence: Source of Chemical Complexity

Giuseppe Cassone[1], Franz Saija[2], Jiri Sponer[1], Judit E. Sponer[1], Martin Ferus[3], Miroslav Krus[4], Angela Ciaravella[5], Antonio Jiménez-Escobar[5], and Cesare Cecchi-Pestellini[5]
[1] Institute of Biophysics of the Czech Academy of Sciences, Královopolská 135, 61265 Brno, Czech Republic; cassone@ibp.cz
[2] CNR-IPCF, Viale Ferdinando Stagno d'Alcontres 37, I-98158 Messina, Italy
[3] J. Heyrovsky Institute of Physical Chemistry, Czech Academy of Sciences, Dolejskova 3, 18223, Prague 8, Czech Republic
[4] Institute of Plasma Physics, Czech Academy of Sciences, Za Slovankou 1782/3, 18200 Prague, Czech Republic
[5] INAF—Osservatorio Astronomico di Palermo, Piazza del Parlamento 1, I-90134 Palermo, Italy; cesare.cecchipestellini@inaf.it
Received 2018 July 31; revised 2018 September 26; accepted 2018 September 28; published 2018 October 16

Abstract

In addition to the manufacture of complex organic molecules from impacting cometary and icy planet surface analogs, which is well-established, dust grain–grain collisions driven by turbulence in interstellar or circumstellar regions may represent a parallel chemical route toward the shock synthesis of prebiotically relevant species. Here we report on a study, based on the multi-scale shock-compression technique combined with ab initio molecular dynamics approaches, where the shock-wave-driven chemistry of mutually colliding isocyanic acid (HNCO) containing icy grains has been simulated by first principles. At the shock-wave velocity threshold triggering the chemical transformation of the sample (7 km s^{-1}), formamide is the first synthesized species, thus being the springboard for the further complexification of the system. Also, upon increasing the shock impact velocity, formamide is formed in progressively larger amounts. More interestingly, at the highest velocity considered (10 km s^{-1}), impacts drive the production of diverse carbon–carbon bonded species. In addition to glycine, the building block of alanine (i.e., ethanimine) and one of the major components of a plethora of amino acids including, e.g., asparagine, cysteine, and leucine (i.e., vinylamine), have been detected after shock compression of samples containing the most widespread molecule in the universe (H_2) and the simplest compound bearing all of the primary biogenic elements (HNCO). The present results indicate novel chemical pathways toward the chemical complexity typical of interstellar and circumstellar regions.

Key words: astrochemistry – ISM: molecules – molecular processes – shock waves

1. Introduction

Interstellar turbulence, because it is generally supersonic, creates in the interstellar medium (ISM) a texture of low-velocity shocks and localized intense vortices (Hennebelle & Falgarone 2012), which may affect dust evolution more frequently and more significantly than the faster supernovae shock waves. Cycled continuously through a variety of physical conditions, dust grains experience growth mechanisms and processes that redistribute grain mass into units of smaller size, or even entirely remove the solid component.

Relative grain–grain motions arising from magnetohydrodynamic (MHD) turbulence are discussed by, for example, Yan et al. (2004). The turbulent acceleration is modeled as the acceleration due to a spectrum of MHD waves, decomposed into incompressible Alfvénic modes and compressible magnetosonic modes. While the fluid motions accelerate grains through hydrodynamic drag due to the frictional interaction with the gas, electromagnetic fluctuations provide energy exchange involving resonant interactions between the particles and the waves, such as gyroresonance (Yan & Lazarian 2003) and transit accelerations. In particular, the gyroresonance mechanism can accelerate grains to supersonic speed relative to the gas.

The effects of supersonic motions on dust grains may be relevant for chemistry, the most obvious example of this being the accumulation of ice mantles on the surfaces of dust grains. Because dust grains move fast through the turbulent interstellar gas, the accretion process may be powered, providing significant effects upon the distribution of molecular species both in the solid and gas phases (Ge et al. 2016). Low-velocity grain collisions may also have dramatic chemical consequences by triggering grain mantle explosions (e.g., Caselli et al. 1997; Cecchi-Pestellini et al. 2004; Guillet et al. 2011).

When two particles collide at sufficiently high velocity, strong shock waves are driven within them, compressing matter to very high pressures. Such an event induces chemical variations of the initial constituents (Goldman et al. 2010; Martins et al. 2013). If the colliding particles are covered with icy mantles, shock waves may significantly increase the complexity of the ice composition. Turbulence may also drive fragmentation, erosion, and shattering (e.g., Caselli et al. 1997). The threshold velocities for grain–grain shattering are of the order of 1 km s^{-1}. Shattering events can occur over timescales comparable to the collision time (e.g., $\Delta t \approx 1$ ps for vaporization; Tielens et al. 1994), so the chemistry may be already relaxed, and the products of the chemical reactions taking place during the collisions are eventually ejected into the gas phase.

Many organic molecules of moderate complexity, such as ethanol and glycolaldehyde, are detected at relatively high abundances in various interstellar locations, especially in regions of star formation (Herbst & van Dishoeck 2009; Williams & Viti 2014), and are considered to be related to astrobiology. Such species cannot be readily formed by conventional interstellar gas-phase chemistry, and are thought to form through a chemistry involving dust grains. It is known that fairly simple molecular ices accumulating on the surfaces of dust grains in dense gas in star-forming regions transform into relatively complex gas-phase species. This is thought to occur in some form of solid-state chemistry, involving various radicals trapped in the grain mantles, when activated by heating

of the accreting central protostar (e.g., Garrod et al. 2008; Garrod 2013; Cuppen et al. 2017). All of these processes can be replicated in laboratory experiments.

The dominant role of grain surface chemistry has been challenged observationally in cold environments (e.g., Marcelino et al. 2007; Jiménez-Serra et al. 2016). Moreover, Enrique-Romero et al. (2016) have theoretically suggested that the combination of radicals trapped in amorphous water ice (the major component of interstellar ices) may not result in larger molecules. Other theoretical studies propose that complex organic molecules may be formed via suitable gas-phase reaction routes (e.g., Kahane et al. 2013; Skouteris et al. 2017). Still, laboratory experiments show that processing interstellar ice analogs may lead to the formation of complex organic molecules via energetic (e.g., Muñoz Caro et al. 2002; Öberg et al. 2009; Chen et al. 2013) and non-energetic (e.g., hydrogenation of CO and other small radicals; Fedoseev et al. 2015, 2017; Chuang et al. 2016) routes, while recombination of radicals may occur on the fly in the transient high-density gas phase during non-canonical mantle explosions (Rawlings et al. 2013).

Thus far, amino acids have not been identified in the ISM. However, a few species with the peptide moiety have been detected (e.g., formamide, NH_2CHO), perhaps the most important for proteins. The role played by formamide in the emergence of terrestrial life is one of the hottest subjects of contemporary research on the origins of life (Fiore & Strazewski 2016; Sponer et al. 2016a). Formamide may serve as a universal feedstock molecule both for the one-pot (Saladino et al. 2015) as well as for the multistep high-yield (Becker et al. 2016) synthesis of nucleosides. Such species may have also contributed to the formation of nucleobases during extraterrestrial impacts on the early Earth (Ferus et al. 2015). Moreover, in silico simulations of the Miller experiment revealed that formamide plays the role of a key intermediate in the reaction pathway (Saitta & Saija 2014). While formamide is readily formed in interstellar ice analogs (e.g., Jones et al. 2011 and references therein), its gas-phase synthesis has also been suggested (Kahane et al. 2013; Barone et al. 2015). Possible support for this new chemical scenario may come from the observations of formamide emission in a shocked region around a solar-type protostar (Codella et al. 2017). However, Quénard et al. (2018) have shown that either gas-phase formation or grain surface synthesis may dominate depending on the physical conditions of the source. Consequently, both formation routes may possibly co-exist.

Related to formamide is isocyanic acid (HNCO), formally the dehydrogenation product of the simplest amide, which—along with its structural isomer cyanic acid—represents the smallest stable molecule containing all four primary biogenic elements. This species has been observed in a variety of Galactic and extragalactic environments (e.g., López-Sepulcre et al. 2015 and references therein), as well as in processed interstellar icy analogs (Jiménez-Escobar et al. 2014; Fedoseev et al. 2015; Kaňuchová et al. 2016). A recent combined experimental-theoretical study has investigated the HNCO-based synthesis of formamide in exotic planetary atmospheres (Ferus et al. 2018).

In this Letter we explore the chemical processes relevant to colliding HNCO-containing icy grains, whose motions are driven by turbulence in interstellar or circumstellar regions. We simulate the event through uni-axial shock waves described by the multi-scale shock-compression simulation technique (MSST; Reed et al. 2003). The evolving chemistry is then followed exploiting ab initio molecular dynamics (AIMD) approaches.

2. Model and Methods

Laboratory simulations suggest that a very rich chemistry may occur in molecular ices on dust surfaces. The wide range of products hints at the operation of a radical–radical association chemistry, even though mechanistic details of the processing are still largely unknown.

The formation of HNCO in ices proceeds through reaction between CO molecules and radical intermediates involved in the formation of NH_3, i.e., NH and NH_2 (Fedoseev et al. 2015). The formation of isocyanic acid competes with the formation of ammonia in non-polar CO ices, and becomes the favored channel when the atomic hydrogen accretion rate is slow. Ultraviolet photo-processing of water ices containing nitrogen-bearing species may lead to the HNCO synthesis (Jiménez-Escobar et al. 2014). At low temperatures other energetic processing of nitrogen-containing solid mixtures of various compositions drive the synthesis of formamide together with isocyanic acid (e.g., Kaňuchová et al. 2016).

When the densities are high enough for CO to freeze out onto grains, molecular hydrogen is by far the most abundant hydrogen-bearing gas-phase species in dense regions. While H_2 is not expected to accrete firmly onto substrates at temperatures larger than $\approx$7 K, it can be trapped in the micropores of CO ice. Upon investigating thermal- and photo-desorption of CO ices, Muñoz Caro et al. (2010) observed that molecular hydrogen desorbed from the ice at the beginning of the warm-up process ($\approx$8 K). The desorption reached a maximum at 14 K and was completed at 20 K. A possible interpretation for this observation is that H_2 is moving around by quantum tunneling in the amorphous CO ice. Thus, in cold regions H_2 would not only be transiently deposited on the ice surface, it would also accumulate in the bulk. Although in standard conditions H_2 molecules have a low reactivity compared to atomic hydrogen, during compressions this turns out not to be the case.

The great advantage of computations when complementing experiments is that they provide information on selected single molecules and chemical reactions (e.g., Sponer et al. 2016b; Cassone et al. 2018). In this Letter, we have deployed numerical calculations to follow the chemical evolution of a mixture of isocyanic acid and molecular hydrogen when the constituent icy mantle is abruptly subjected to extreme pressures caused by grain–grain collisions in space conditions. A sample composed by 32 HNCO and 50 H_2 molecules (i.e., 228 atoms) is simulated by means of Density Functional Theory–based Born–Oppenheimer molecular dynamics exploiting the CP2K molecular simulation software (Hutter et al. 2014). The starting simulation boxes (i.e., the super-cells) have been prepared such that the internal pressure—determined by means of first-principles evaluation of the stress tensor—were equal to 5 GPa. As usual, all of the structures were replicated in space by means of periodic boundary conditions. We used a plane-wave cutoff of 400 Ry and optimized triple zeta valence polarized basis set for all elements in the system. Goedecker–Teter–Hutter pseudopotentials (Goedecker et al. 1996), along with the D3(BJ) (Grimme et al. 2010, 2011) dispersion-corrected

Perdew–Burke–Ernzerhof (Perdew et al. 1996) exchange and correlation functional, have been employed.

Shock waves are described by means of the MSST (Reed et al. 2003). This approach relieves typical system-size issues, at the same time allowing for a realistic description of chemistry under extreme conditions (Goldman et al. 2010). Each molecular dynamics step, corresponding to 0.5 fs of dynamics, required about 100 s in order to be completed on a computer cluster exploiting, for each simulation carried out, 32 Intel ES 4650 processors and optimized inter-node ultra-fast communications (i.e., InfiniBand FDR10 Mellanox). After compression of the sample, a decompression of the simulation boxes enables the identification of the "stable" products stemming from the impact-induced chemical reactions. We have tested uni-axial shock-wave velocities ranging from 6 to 10 km s^{-1}. This way, shock-compressed thermodynamic states identifiable with pressures $P_S = 37$ GPa (6 km s^{-1}), 49 GPa (7 km s^{-1}), 58 GPa (8 km s^{-1}), 65 GPa (9 km s^{-1}), and 72 GPa (10 km s^{-1}) are generated through the MSST within dynamical timescales of about 5–10 ps. Then, a decompression process of the simulation boxes follows the maximally compressed state of each simulation cell, leading each system to a final decompressed pressure of about 5 GPa, corresponding to the unperturbed (starting) simulation cell. Unless explicitly specified, all of the chemical yields refer to the initial amount of HNCO molecules.

Simulation of the global process of decompression, as well as that of the "decompressed" states, is performed for times longer than 20 ps. These timescales allow for the evaluation of the (meta)stable species in each system by means of direct inspection of the trajectories. The atomic radial distribution functions (RDFs) have been especially useful for following the systematic increase of molecular complexity as a function of increasing shock-wave velocities. RDFs describe how the density of a specific particle varies as a function of distance from a reference particle. More precisely, they represent the average densities of particles (atoms, molecules, etc.) at the position r, given that a tagged particle (atom, molecule, etc.) is at a pre-selected origin (Allen & Tildesley 1997); operationally, RDFs have been determined as three-dimensional histograms over the particles' labels averaged over time and space. Thus, numerical results are referred to the "decompressed" state of the simulation box, which is achieved after the relaxation of the compressed state. Finally, each decompression process starts from the nominal Hugoniot temperature of each given shock-compressed state and is conducted at several temperatures in the range 300–2500 K in order to check for eventual temperature-dependent chemical reactions after each compressed state. It turned out that, notwithstanding a trivial enhancement of the molecular vibrations, no differences in the final composition of the products has been recorded for different temperature values, proving a posteriori that all of the chemical transformations are pressure-driven reactions. To this aim, distinct Car–Parrinello (Car & Parrinello 1985) molecular dynamics simulations with the Parrinello–Rahman Lagrangian (Parrinello & Rahman 1980) for the motion of the simulation box are performed by means of the plane-wave/pseudopotentials software package Quantum ESPRESSO (Giannozzi et al. 2009) in order to independently reproduce the decompression process of the simulation super-cells. In these cases, the fictitious electronic masses are set to a value of 300 au, with a cutoff energy of 40 Ry, and a cutoff energy for the charge density of 320 Ry, which allowed us to adopt a timestep of 0.12 fs. In all cases, the dynamics of nuclei is simulated classically using the Verlet algorithm.

Although CO in icy mantles may in principle be involved in the overall chemistry here described, due to the substantial computational demand of the calculations (i.e., ≈350000 CPU hours), we will consider the inclusion of this molecule in a future work. In this way, it will be possible, inter alia, to discern not only how the overall reaction network is affected by the presence of CO but also how each reaction pathway is inhibited/catalyzed by the presence of such a species. Additionally to these considerations, another rationale holds for the insertion of water molecules to the initial samples. In fact, CO ice in the interstellar medium is mainly found on top of pre-existing H_2O icy layers (e.g., Pontoppidan et al. 2008), and hence it is expected to be shock-compressed on timescales of the order $\Delta t \gtrsim w/v_d$, w being the icy mantle thickness. For $v_d = 10$ km s^{-1}, and $w \approx 10$ nm, we obtain $\Delta t \gtrsim 1$ ps, sizably longer than those characterizing the initial chemical activity that takes place in presence of HNCO and H_2 on the surface. Moreover, as it will be laid out in the next section, since water is copiously produced at the most intense shock regime, the latter species is somehow involved in the post-collision chemistry in the respective sample.

3. Results

Averaged molecular correlations can be quantified by means of the RDFs (Hansen & McDonald 2013). Moreover, by sampling shorter atom-to-atom distances, important intra-molecular insights can be earned in determining these structural functions.

We have not observed any chemical activity when subjecting the mixture of HNCO and H_2 to a uni-axial shock wave propagating at 6 km s^{-1}. In the highly compressed state, when pressures reach 37 GPa (Hugoniot temperature $T_H = 857$ K), some strong inter-molecular interactions between HNCO molecules are evidenced; once the system is left to relax, no reaction products are detected.

The situation changes significantly when the impact velocity exceeds 7 km s^{-1}, generating peak pressures equal to or higher than 49 GPa ($T_H \geqslant 1213$ K). After decompression we observed the formation of formamide and carbamoyl isocyanate ($H_2NCONCO$). Although the amount of the newly formed products is relatively low (about 3% of the initial HNCO content) it suggests that formamide is the first compound synthesized from a sample of HNCO and H_2. As shown in Figure 1, the first peak of the hydrogen–hydrogen RDF clearly decreases with increasing pressure. This indicates that the amount of H_2 converted into more complex species increases when the system is subjected to progressively more intense shock impacts. It is interesting to note that in shocks impacting on interstellar and circumstellar regions, the formation of species relying on endothermic reactions is enhanced by several orders of magnitude as the shock velocities increases to over 7 km s^{-1} (Lesaffre et al. 2013). Furthermore, similar impact velocities are required to explain the observed excitation of the pure rotational lines of H_2 (e.g., Godard et al. 2014). At the maximum considered pressure ($P_S = 72$ GPa, $v_d = 10$ km s^{-1}), after decompression only 4% of the initial amount of H_2 remains in unreacted form, which is reflected in the RDFs (see Figure 1) by a reduction of the intensity of the typical sharp first peak located at 0.76 Å.

Table 1
Inventory of Species Formed in the Impact Simulations under Various Conditions

P_S (GPa) | T_H (K) | v_d (km s^{-1})					
5 |−| 0	37 |857| 6	49 |1213| 7	58 |1550| 8	65 |1837| 9	72 |2122| 10
H_2	H_2	H_2	H_2	H_2	H_2
HNCO	HNCO	HNCO	HNCO	HNCO	CO_2
		H_2NCHO	H_2NCHO	H_2NCHO	H_2O
		$H_2NCONCO$	$H_2NCONCO$	$H_2NCONHCHO$	NH_3, NH_4^+
				$H_2NCONHCOO^-$	HCN, CN^-
				H_2NCOO^-, H_3NCHO^+ complex	HCOOH
					H_2NCHO
					CH_2CHOH
					H_2NCOOH
					CH_2NH
					CH_3NH_2
					NH_2CH_2COOH
					CH_3CHNH
					CH_2CHNH_2
					$HNC(NH_2)_2$ complex
					C–N aliphatic chains

Note. P_S: maximum pressure reached in the simulation; T_H: maximum temperature reached; v_d: velocity of the uni-axial shock wave.

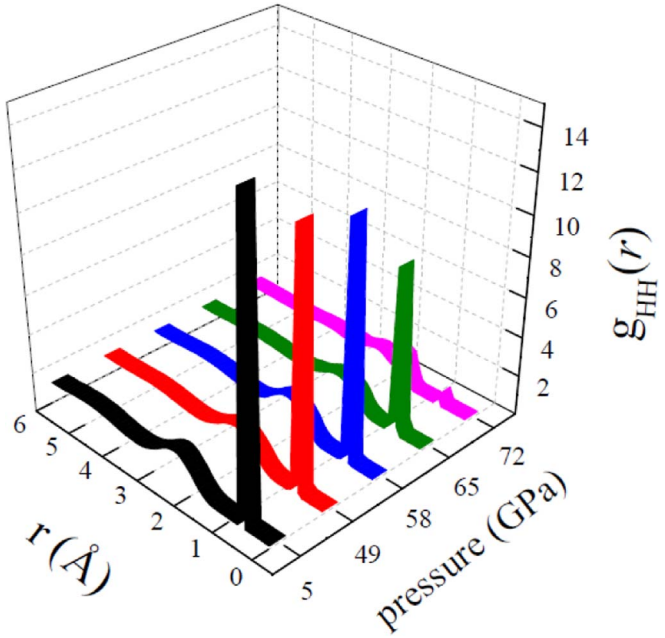

Figure 1. Hydrogen–hydrogen RDF for different shock pressures, determined after decompression of the simulation boxes.

In Table 1 we provide an inventory of the species formed in our simulations performed assuming various uni-axial shock-wave velocities. A shock pressure of 58 GPa ($T_H = 1550$ K) induces the formation of formamide and carbamoyl isocyanate, with each product representing about the 6% of the original amount of HNCO (twice the case of $P_S = 49$ GPa). At $P_S = 65$ GPa (or $v_d = 9$ km s^{-1}), the amount of synthesized formamide jumps to 16% of the original HNCO content. At this pressure other products, such as formylurea ($H_2NCONHCHO$, 3%) and allophanate ($H_2NCONHCOO^-$, 3%), start to form in detectable concentrations, together with C–N containing aliphatic chains that exhibit carbamate (H_2NCOO^-) and formylazanium (NH_3CHO^+) groups.

As shown in Figure 2 (top panel), upon reaching the shock pressure of 65 GPa an intra-molecular peak rises in the oxygen–hydrogen RDF at about 1 Å, which becomes absolutely dominant at 72 GPa. The peak can be assigned to the formation of water (38%), formic acid (HCOOH, 3%), glycine (NH_2CH_2COOH, 3%), carbamic acid (NH_2COOH, 3%), and vinyl alcohol (CH_2CHOH, 3%). Remarkably, this is accompanied with the onset of a new peak at 1.16 Å on the carbon–nitrogen RDF above 65 GPa (Figure 2, middle panel) which is associated with the formation of HCN and CN^- species. At the highest shock pressures investigated, a shoulder in the carbon–oxygen RDF at about 2.35 Å suggests formation of glycine and vinyl alcohol (Figure 2, bottom panel). The fact that many species exhibit similar yields is due to the statistically exiguous number of molecules of the starting numerical sample which is, however, typical of high-demanding AIMD simulations.

The presence of some aliphatic chains containing C–N is underlined by the onset of novel first peaks in the carbon–carbon RDF characterizing the sample subjected to a shock wave producing a maximum pressure of 65 GPa. In particular, as shown in Figure 3, two first peaks rise up in the relative C–C RDF, whereas just a small first peak can be recognized in the C–C RDF for shock pressures equal to 49 GPa and 58 GPa (which, in such cases, is ascribable to the presence of carbamoyl isocyanate). In addition, as listed in Table 1, an interesting guanidine-containing complex has been synthesized at 72 GPa.

Finally, a striking result is the onset of many C–C covalent bonds once the system is relaxed to standard pressures after being shock-compressed up to 72 GPa by a shock wave propagating at 10 km s^{-1}. This is evidenced by the impressive first peak located at 1.35 Å in Figure 3, which represents the signature of the birth of new C–C bonded species in the sample. In addition to the already mentioned glycine and vinyl alcohol, the syntheses of ethanimine (CH_3CHNH, 3%) and its tautomeric form, vinylamine (CH_2CHNH_2, 3%), have also been observed. Whereas the former is the building block of alanine, the latter is one of the major components of a vast

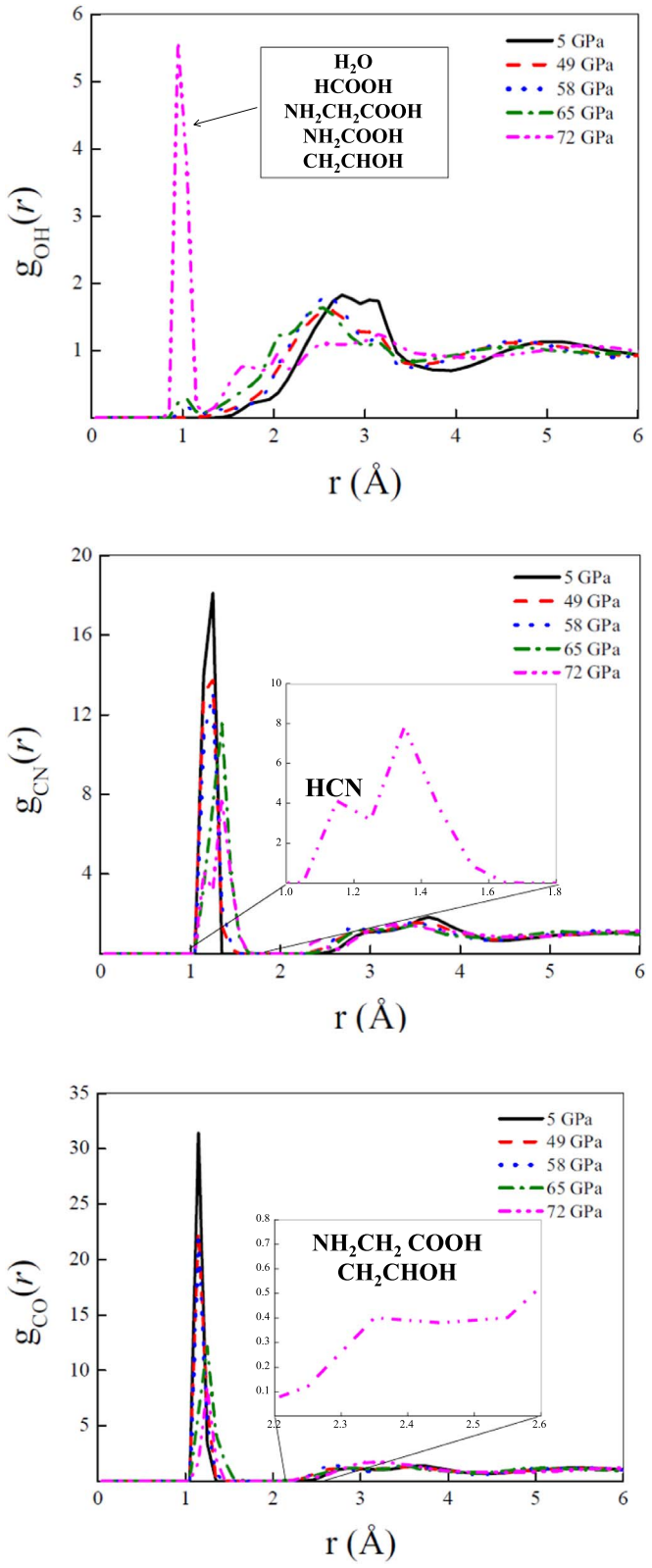

Figure 2. RDFs for oxygen–hydrogen (top panel), carbon–nitrogen (middle panel), and carbon–oxygen (bottom panel) atom pairs. Labels indicate the peak pressure reached at the impact. Whereas the inset of middle panel magnifies the peaks associated with the formation of HCN and CN^-, the inset of the bottom panel highlights a shoulder in the RDF indicating the onset of glycine and vinyl alcohol at the highest shock velocity.

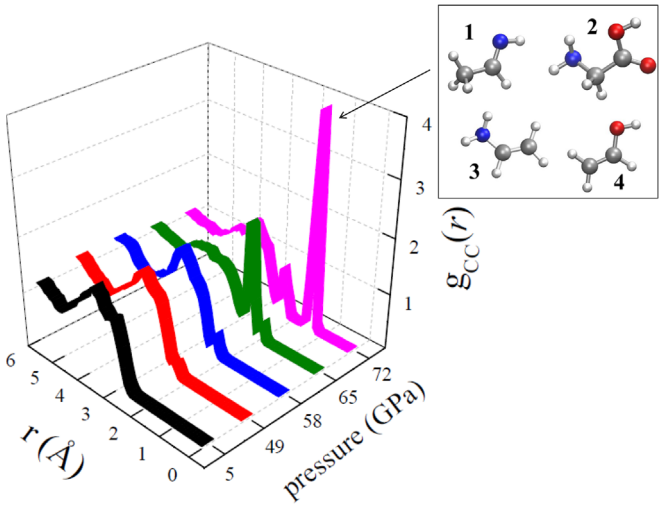

Figure 3. C–C RDFs for different shock pressures and determined after decompression of the simulation boxes. The onset of the peak at 1.35 Å is due to the presence of ethanimine (1), glycine (2), vinylamine (3), and vinyl alcohol (4) (see the inset).

series of amino acids: asparagine, aspartic acid, cysteine, leucine, phenylalanine, serine, and tyrosine.

Upon intense compression, a molecular system typically achieves transient inter-molecular distances that instantaneously generates the formation of exotic short-lived polymers and complexes. At $P_S = 72$ GPa a pseudo-glycine-containing complex has been observed, partially resembling those detected by Goldman et al. (2010). However, a stable glycine is synthesized in our sample by following the reaction pathway depicted in Figure 4. In particular, soon after the beginning of the decompression process a short-lived (100 fs) anion receives a proton, initially from H_3O^+, and then from the ammonium ion NH_4^+. In a few hundreds of fs the glycine anion is neutralized by a further proton transfer, occurring through a nearby water molecule (which, in turn, will be rapidly neutralized), eventually leading to a stable glycine molecule.

One potential problem in our description might be the destruction of the ice layer upon impact. Shattering occurs on mechanical timescales, the latter of the order of the collision time. To derive such a time, we use the Rayleigh (1906) estimate for collisions without adhesion $t_c \approx 5 \times (c_s/v_d)^{0.2}(A/c_s)$ (Chokshi et al. 1993), with c_s the sound speed, and $A = a_1a_2/(a_1 + a_2)$ the reduced radius in the impact. As the speed of sound in ice is nearly three times faster than in water, i.e., $c_s \approx 4\,\mathrm{km\,s^{-1}}$, considering the impact between particles of the same size a we obtain $t_c \approx 825 \times (a/1\,\mu\mathrm{m})\ (v_d/1\,\mathrm{km\,s^{-1}})^{-0.2}$ ps. For an impact velocity $v_d = 10\,\mathrm{km\,s^{-1}}$, 1 μm-sized grains experience a collision time $t_c \approx 550$ ps, about three orders of magnitude longer than e.g., the formation time of glycine. Because chemical reaction times are of the order of fractions of ps, the mechanical destruction of the ice occurs generally when chemical products are stabilized for a very long time.

H_2 is trapped in micropores of CO (Muñoz Caro et al. 2010) or water (Rowland et al. 1991). Muñoz Caro et al. (2010) found that the early desorption of CO (from 15 to 23 K) might be caused by the release of H_2 molecules from the CO ice. Thus, at least locally, the abundance of H_2 molecules relative to CO is

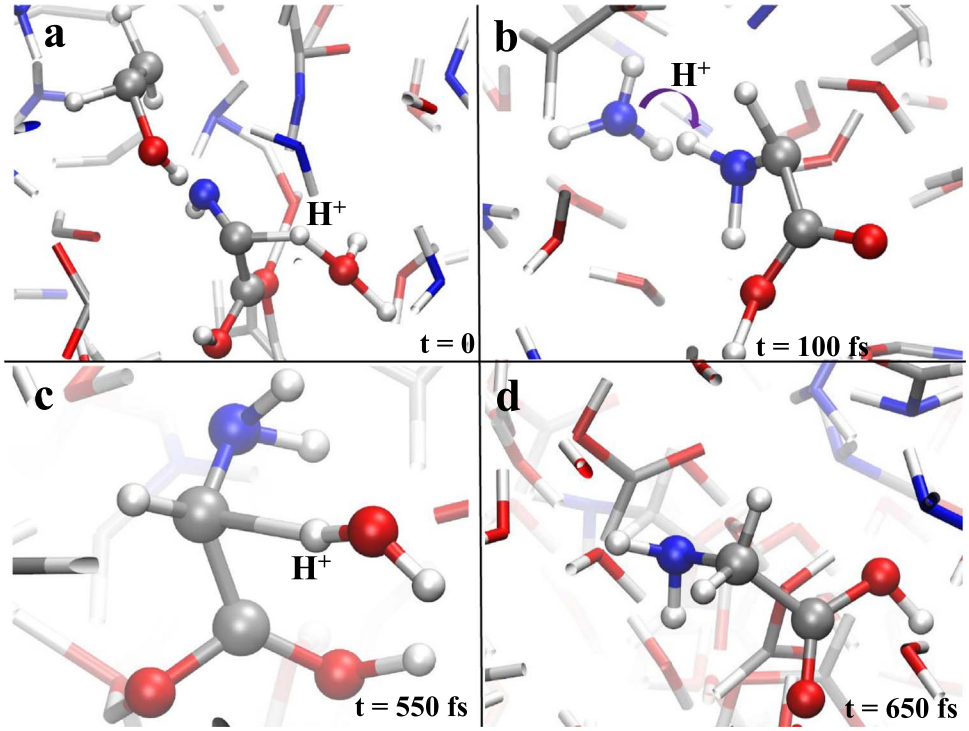

Figure 4. Glycine formation mechanism during the decompression of an HNCO and H_2 mixture where a shock wave propagating at 10 km s^{-1} impacted. Red, silver, blue, and white coloring refers to oxygen, carbon, nitrogen, and hydrogen atoms, respectively. After the compression of the simulation cell, where a pseudo-glycine-containing complex has been observed, a highly ionized glycine anion is transiently detected. After successive proton transfer events due to an hydronium cation (a), an ammonium cation (b), and a water molecule (c), glycine is stably synthesized (d).

substantial. As stated in the previous section, in a future work we shall investigate the role of CO in the ices in the chemistry of grain–grain collisions.

4. Conclusions

We present a new scheme for the synthesis of formamide, glycine, and amino-acid precursors from the shock-wave-induced chemistry of systems composed by isocyanic acid and molecular hydrogen. Our quantum-based investigations indicate that mutually colliding dust grains covered by icy layers are able to produce, at the shock-wave velocity threshold triggering the chemical evolution of the sample, formamide. This, in turn, will be progressively synthesized under the effect of more intense shock compressions. In addition, when shock waves propagating at 10 km s^{-1} impact the sample, the simplest amino-acid, glycine, is spontaneously formed along with ethanimine and vinylamine. The former is the main constituent of alanine, whereas the latter is one of the building blocks of seven distinct amino acids. The mechanism that we propose may be at work in regions in which the level of turbulence is relatively high, such as turbulent diffuse molecular clouds (see, e.g., the detection of formamide by Thiel et al. 2017), and protoplanetary regions. In pre-stellar cores, where the level of turbulence is small ($\lesssim$1 km s^{-1}), collisions are not energetic enough to induce pressure-driven formation of complex organics. However, impacts are still able to provide impulsive heating of the colliding particles, enough to fuel rapid exothermic chemical reactions, leading to a thermal runaway. Such reactions may involve free radicals, whose mobility driven by the warm-up may liberate sufficient energy to explode (Greenberg 1976).

In conclusion, in this Letter we show that conversion from chemical simplicity to chemical complexity can occur very rapidly within the transient events following catastrophic impacts. The proposed mechanism is general and not specific to any single source. Although limited to a particular reactive system, the ubiquity of collisions driven by turbulent motions does indicate that there are astronomical consequences from this idea. One important point is that systems, such as the one that we consider in this Letter, may be the subject of laboratory validation (see e.g., Ferus et al. 2018).

We would like to thank the anonymous referee for comments and suggestions that helped clarify and improve the manuscript.

G.C., J.E.S., and M.F. acknowledge the GACR (Czech Science Foundations) under the grant No. 17-05076S.

This work has been supported by the project PRIN-INAF 2016 The Cradle of Life—GENESIS-SKA (General Conditions in Early Planetary Systems for the rise of life with SKA).

We gratefully acknowledge Munõz Caro and Chen for the enlightening discussion on CO ices.

ORCID iDs

Giuseppe Cassone https://orcid.org/0000-0003-1895-2950
Franz Saija https://orcid.org/0000-0002-5970-9001
Angela Ciaravella https://orcid.org/0000-0002-3127-8078
Cesare Cecchi-Pestellini https://orcid.org/0000-0001-7480-0324

References

Allen, M. P., & Tildesley, D. J. 1997, Computer Simulation of Liquids, Oxford Science Publications (Oxford: Clarendon), 183

Barone, V., Latouche, C., Skouteris, D., et al. 2015, MNRAS, 453, L31
Becker, S., Thoma, I., Deutsch, A., et al. 2016, Sci, 352, 833
Car, R., & Parrinello, M. 1985, PhRvL, 55, 2471
Caselli, P., Hartquist, T. W., & Havnes, O. 1997, A&A, 322, 296
Cassone, G., Sponer, J., Sponer, J. E., et al. 2018, ChCom, 54, 3211
Cecchi-Pestellini, C., Scappini, F., Saija, R., et al. 2004, IJAsB, 4, 287
Chen, Y.-J., Ciaravella, A., Muñoz Caro, G. M., et al. 2013, ApJ, 778, 162
Chokshi, A., Tielens, A. G. G. M., & Hollenbach, D. 1993, ApJ, 407, 806
Chuang, K.-J., Fedoseev, G., Ioppolo, S., van Dishoeck, E. F., & Linnartz, H. 2016, MNRAS, 455, 1702
Codella, C., Ceccarelli, C., Caselli, P., et al. 2017, A&A, 605, L3
Cuppen, H. M., Walsh, C., Lamberts, T., et al. 2017, SSRv, 212, 1
Enrique-Romero, J., Rimola, A., Ceccarelli, C., & Balucani, N. 2016, MNRAS, 459, L6
Fedoseev, G., Chuang, K.-J., Ioppolo, S., et al. 2017, ApJ, 842, 52
Fedoseev, G., Ioppolo, S., Zhao, D., Lamberts, T., & Linnartz, H. 2015, MNRAS, 446, 439
Ferus, M., Laitl, V., Knizek, A., et al. 2018, A&A, 616, 150
Ferus, M., Nevosvorny, D., Sponer, J., et al. 2015, PNAS, 112, 657
Fiore, M., & Strazewski, P. 2016, Angew. Chem. Int. ed., 55, 13930
Garrod, R. T. 2013, ApJ, 765, 60
Garrod, R. T., Widicus Weaver, S. L., & Herbst, E. 2008, ApJ, 682, 283
Ge, J. X., He, J. H., & Yan, H. R. 2016, MNRAS, 455, 3570
Giannozzi, P., Baroni, S., Bonini, N., et al. 2009, JPCM, 21, 395502
Godard, B., Falgarone, E., & Pineau des Forêts, G. 2014, A&A, 570, A27
Goedecker, S., Teter, M., & Hutter, J. 1996, PhRvB, 54, 1703
Goldman, N., Reed, E. J., Fried, L. E., Kuo, I.-F. W., & Maiti, A. 2010, NatCh, 2, 949
Greenberg, J. M. 1976, Ap&SS, 39, 9
Grimme, S., Anthony, J., Ehrlich, S., & Krieg, H. 2010, JChPh, 2010, 154104
Grimme, S., Ehrlich, S., & Goerigk, L. 2011, JChPh, 32, 1456
Guillet, V., Pineau des Forêts, G., & Jones, A. P. 2011, A&A, 527, 123
Hansen, J.-P., & McDonald, I. R. 2013, Theory of Simple Liquids (4th ed.; New York: Academic)
Hennebelle, P., & Falgarone, E. 2012, A&ARv, 20, 55
Herbst, E., & van Dishoeck, E. F. 2009, ARA&A, 47, 427
Hutter, J., Iannuzzi, M., Schiffmann, F., & VandeVondele, J. 2014, Computational Molecular Science, 4, 15
Jiménez-Escobar, A., Giuliano, B. M., Muñoz Caro, G. M., Cernicharo, J., & Marcelino, N. 2014, ApJ, 788, 19
Jiménez-Serra, I., Vasyunin, A., Caselli, P., et al. 2016, ApJL, 830, L6
Jones, B. M., Bennett, C. J., & Kaiser, R. I. 2011, ApJ, 734, 78
Kahane, C., Ceccarelli, C., Faure, A., & Caux, E. 2013, ApJL, 763, L38
Kaňuchová, Z., Urso, R. G., Baratta, G. A., et al. 2016, A&A, 585, A155
Lesaffre, P., Pineau des Forêts, G., Godard, B., Guillard, P., & Boulanger, F. 2013, A&A, 550, 106
López-Sepulcre, A., Jaber, A. A., Mendoza, E., et al. 2015, MNRAS, 449, 2438
Marcelino, N., Cernicharo, J., Agúndez, M., et al. 2007, ApJL, 665, L127
Martins, Z., Price, M. C., Golmand, N., Sephton, M. A., & Burchell, M. J. 2013, NatGe, 6, 1045
Muñoz Caro, G. M., Jiménez-Escobar, A., Martín-Gago, J. Á., et al. 2010, A&A, 522, A108
Muñoz Caro, G. M., Meierhenrich, U. J., Schutte, W. A., et al. 2002, Natur, 416, 403
Öberg, K. I., Garrod, R. T., van Dishoeck, E. F., & Linnartz, H. 2009, A&A, 504, 891
Parrinello, M., & Rahman, A. 1980, PhRvL, 45, 1196
Perdew, J. P., Burke, K., & Ernzerhof, M. 1996, PhRvL, 77, 3865
Pontoppidan, K. M., Boogert, A. C. A., Fraser, H. J., et al. 2008, ApJ, 678, 1005
Quénard, D., Jiménez-Serra, I., Viti, S., Holdship, J., & Coutens, A. 2018, MNRAS, 474, 2796
Rawlings, J. M. C., Williams, D. A., Viti, S., Cecchi-Pestellini, C., & Duley, W. W. 2013, MNRAS, 430, 264
Rayleigh, J. W. S. 1906, PMag, 11, 283
Reed, E. J., Fried, L. E., & Joannopoulos, J. D. 2003, PhRvL, 90, 235503
Rowland, B., Fisher, M., & Devlin, J. P. 1991, JChPh, 95, 1378
Saitta, A. M., & Saija, F. 2014, PNAS, 111, 13768
Saladino, R., Carota, E., Botta, G., et al. 2015, PNAS, 112, E2746
Skouteris, D., Vazart, F., Ceccarelli, C., et al. 2017, MNRAS, 468, L1
Sponer, J. E., Sponer, J., Novakova, O., et al. 2016a, E. Chem. Eur. J., 22, 3572
Sponer, J. E., Szabla, R., Góra, R. W., et al. 2016b, PCCP, 18, 20047
Thiel, V., Belloche, A., Menten, K. M., Garrod, R. T., & Müller, H. S. P. 2017, A&A, 605, L6
Tielens, A. G. G. M., McKee, C. F., Seab, C. G., & Hollenbach, D. J. 1994, ApJ, 431, 321
Williams, D. A., & Viti, S. 2014, Observational Molecular Astronomy: Exploring the Universe Using Molecular Line Emissions (Cambridge: Cambridge Univ. Press)
Yan, H. R., & Lazarian, A. 2003, ApJL, 592, L33
Yan, H. R., Lazarian, A., & Draine, B. T. 2004, ApJ, 616, 895